Supporting Information

Direct Laser Patterning and Phase Transformation of 2D $PdSe_2$ Films for On Demand Device Fabrication

Viktoryia Shautsova,[1*] Sapna Sinha,[1] Linlin Hou,[1] Qianyang Zhang,[1] Martin Tweedie,[1] Yang Lu,[1] Yuewen Sheng,[1] Benjamin Porter,[1] Harish Bhaskaran,[1] Jamie Warner[1*]

Department of Materials, University of Oxford, Parks Road, Oxford OX1 3PH, United Kingdom

*email: Jamie.warner@materials.ox.ac.uk, viktoryia.shautsova@materials.ox.ac.uk

Contents

S1. Crystal analysis of Pd nanoparticles

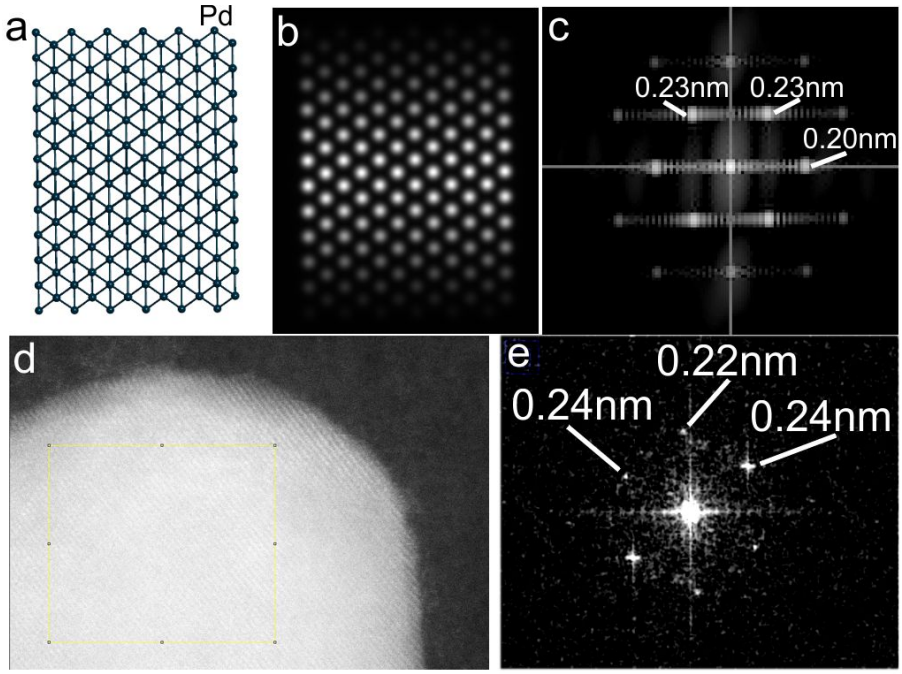

Figure S1. (a) Atomic model of the Pd crystal. (b) STEM image simulation of the atomic model presented in (a). (c) FFT of the simulation in (b) showing crystal spacing. (d) ADF-STEM image of the Pd nanoparticle and corresponding FFT (e) with crystal spacing indicated. We attribute the minor differences in crystal spacing to scan drift observed during imaging.

S2. Laser-induced $Pd_{17}Se_{15}$ phase

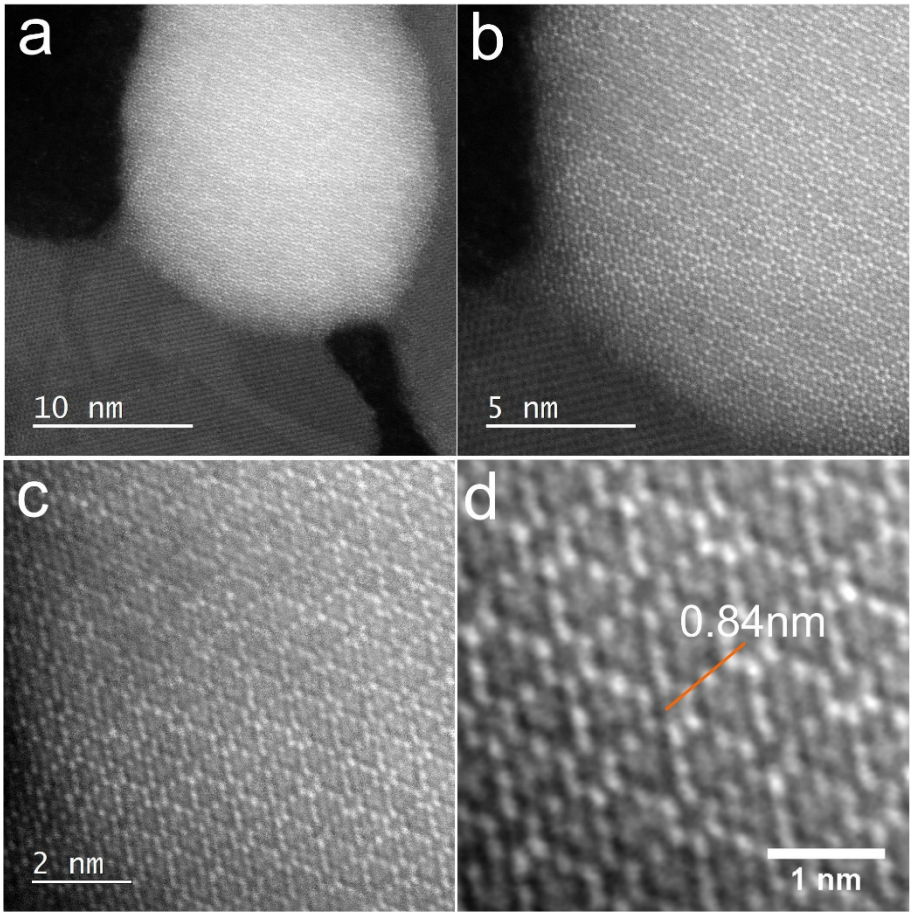

Figure S2.1. STEM characterization of crystal structure of laser-induced $Pd_{17}Se_{15}$ phase. (a) Low magnification ADF-STEM of the material after laser exposure with 3 mW power and 5 µm laser spot. (b-d) Magnified ADF-STEM image of the laser-modified material.

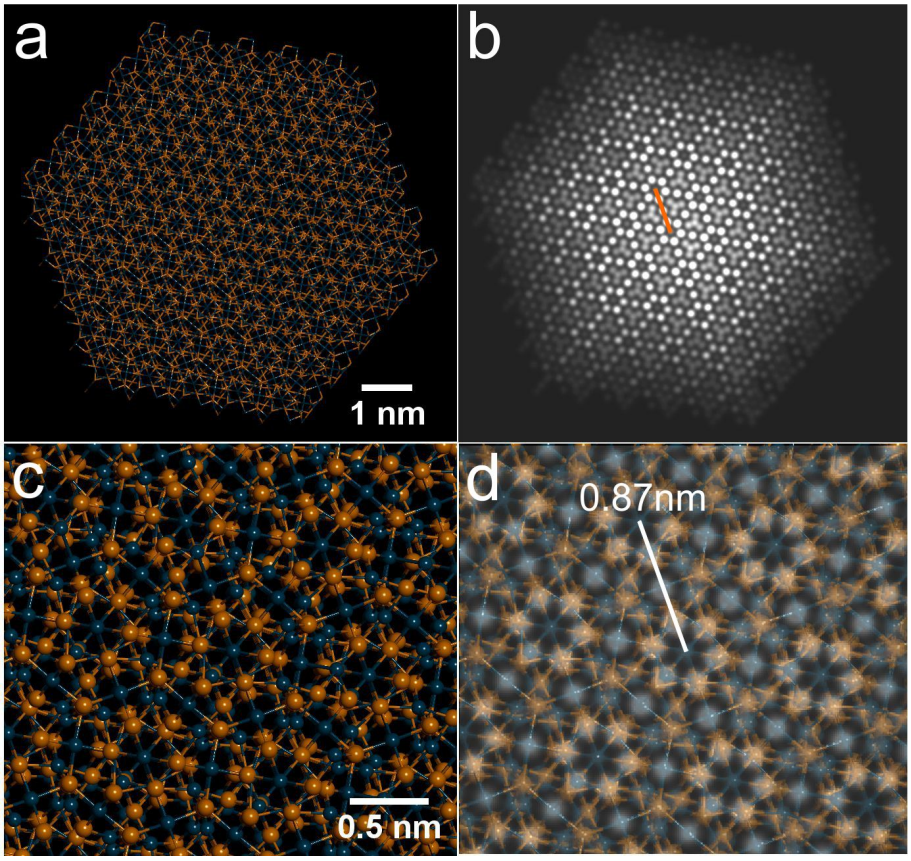

Figure S2.1. (a) Atomic model of the $Pd_{17}Se_{15}$ phase. (b) STEM image simulation of the atomic model presented in (a). (c) Magnified atomic model of the $Pd_{17}Se_{15}$ phase. (d) Overlay of the atomic model presented in (c) and corresponding STEM image simulation.

S3. AFM measurements of the film thickness

To measure the $PdSe_2$ thickness, the film was analysed in 5 positions widely separated from each other to ensure the uniformity of the film thickness. The average film thickness of ~5.5 nm is extracted. Figure S2 (a) shows a typical AFM image of the film edge and corresponding cross-section used to extract the film thickness. Taking into account a typical thickness of a $PdSe_2$ monolayer of 0.4 nm, we can estimate that the $PdSe_2$ film contains ~14 layers. It should be noted that this estimate provides the upper limit due to additional thickness induced by polymer residues present on the surface and by the gap between the film and the underlying substrate.

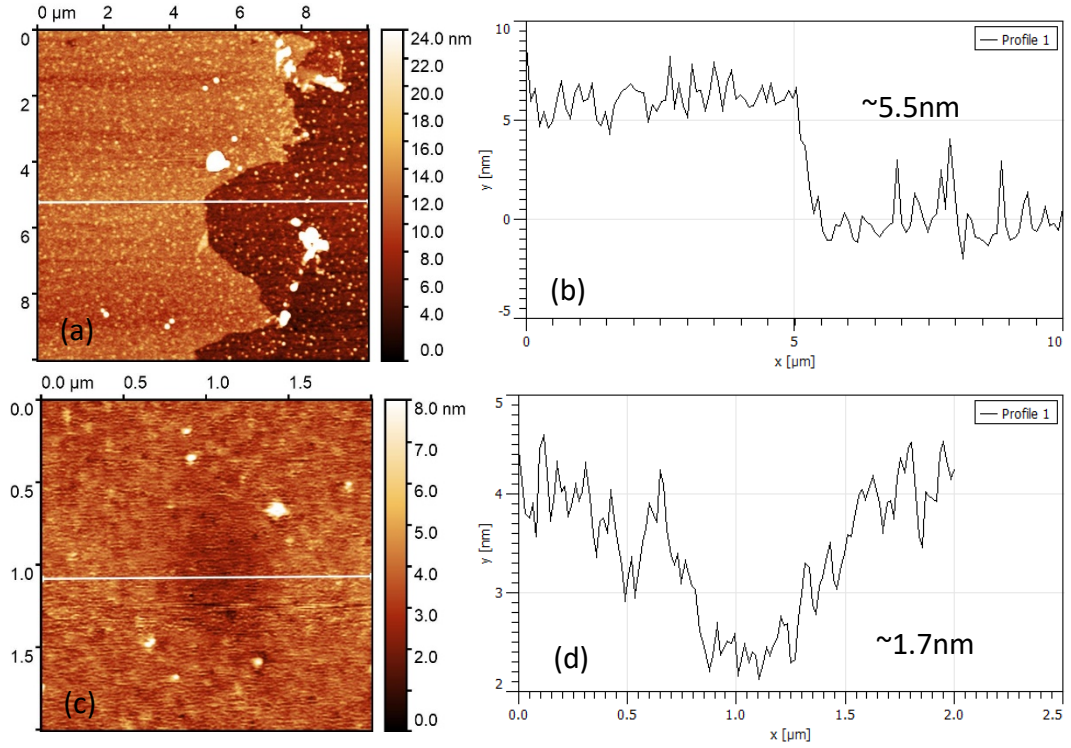

Figure S3. AFM measurements of $PdSe_2$ fillm. (a, b) AFM measurements of the film thickness. (c, d) AFM measurements of the $PdSe_2$ film after exposure to 1.8 mW, as discussed in the main text.

S4. SEM images of material degradation

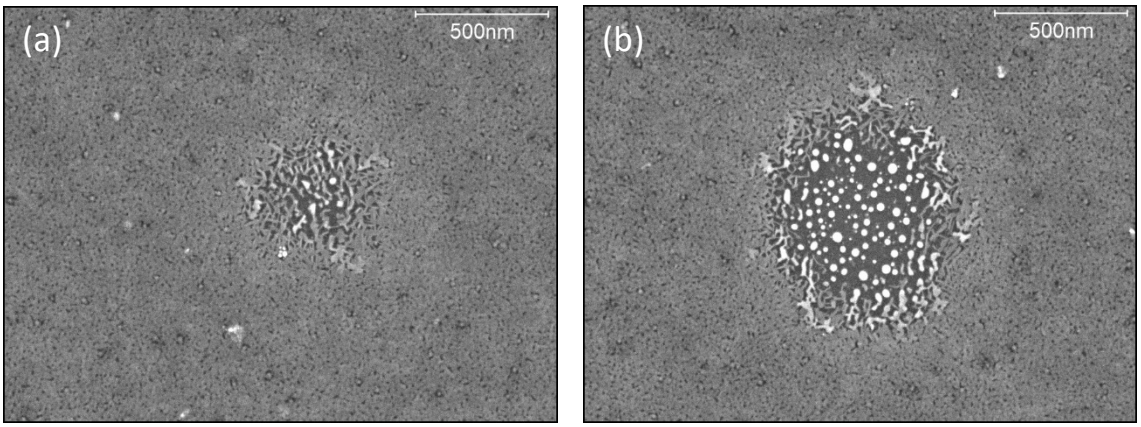

Figure S4. SEM images of the $PdSe_2$ exposed for 1 s with 3.5 mW (a) and 7.8mW (b) laser power.

S5. SEM images of material patterning with 3.5 mW laser power

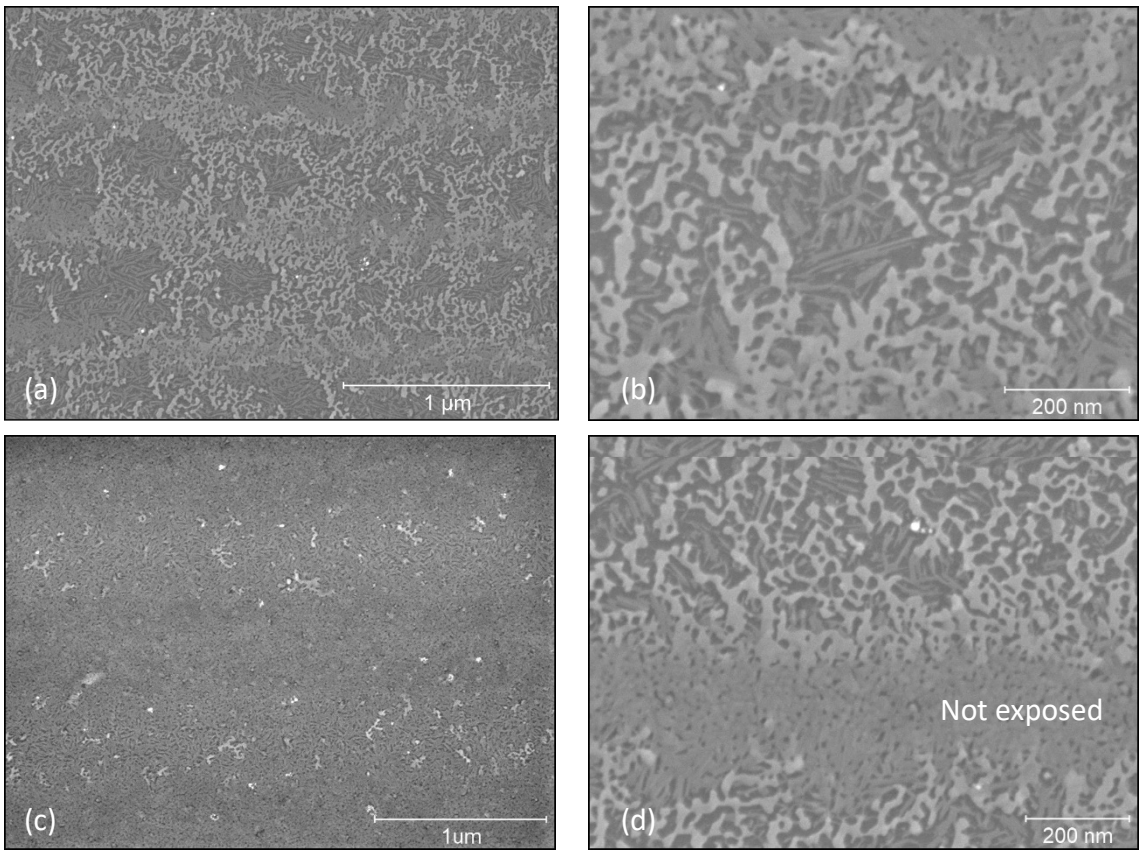

Figure S5. SEM images of the $PdSe_2$ exposed for 1 s with 3.5 mW. The scanning conditions are as following: (a) 500 nm step in x direction and 500 nm step in y direction and (b) 500 nm step in x direction and 1000 nm step in y direction.

S6. Additional EDX and Raman spectral data

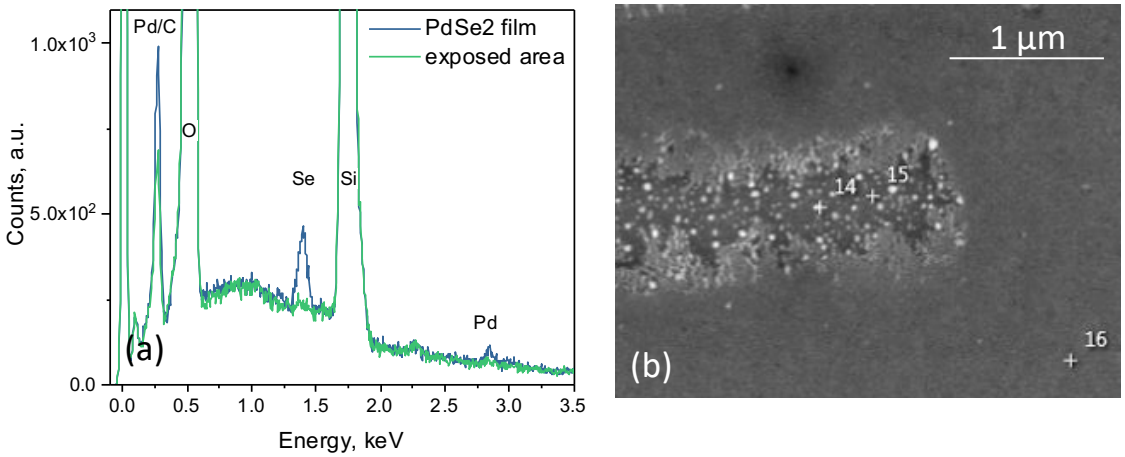

Figure S6.1. EDX spectroscopy of the $PdSe_2$ material degradation after laser patterning performed with 7.8 mW power and 500nm step as discussed in the main text. (a) EDX spectra of the initial film (N16 in (b)) and the exposed region after

patterning (N15 in (b)). (b) SEM image of the analysed region with the crosses indicating positions of spectra collection.

To further study the Raman modes transitions for the phase transformation of $PdSe_2$, we performed extra measurements to study of the $PdSe_2$ layer that was thermally annealed at 450C to promote full phase transformation from $PdSe_2$ to $PdSe_{2-x}$, as confirmed by STEM [1]. Again, our results demonstrate negligible change of the HF Raman modes.

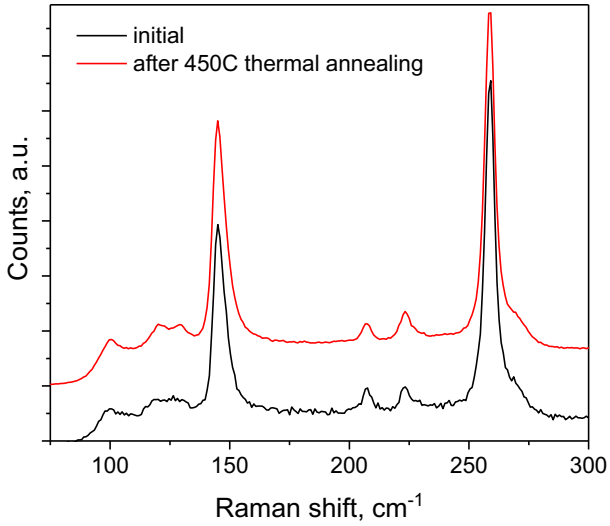

Figure S6.2. Raman spectroscopy of the $PdSe_2$ material after thermal annealing at 450C that results in phase transformation from $PdSe_2$ to $PdSe_{2-x}$, as discussed in details in our previous work Ref. [1].

To further confirm high quality of graphene used for the electrode fabrication, we performed Raman spectroscopy characterisation after the electrode patterning.

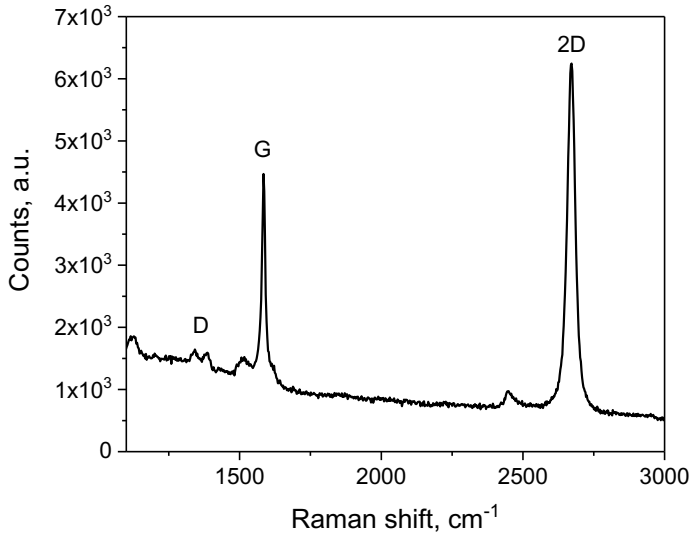

Figure S6.3. Raman spectroscopy of graphene demonstrating high intensity ratio between the 2D and G peaks and low intensity of the D peak.

S7. AFM and SEM measurements of the devices after laser annealing

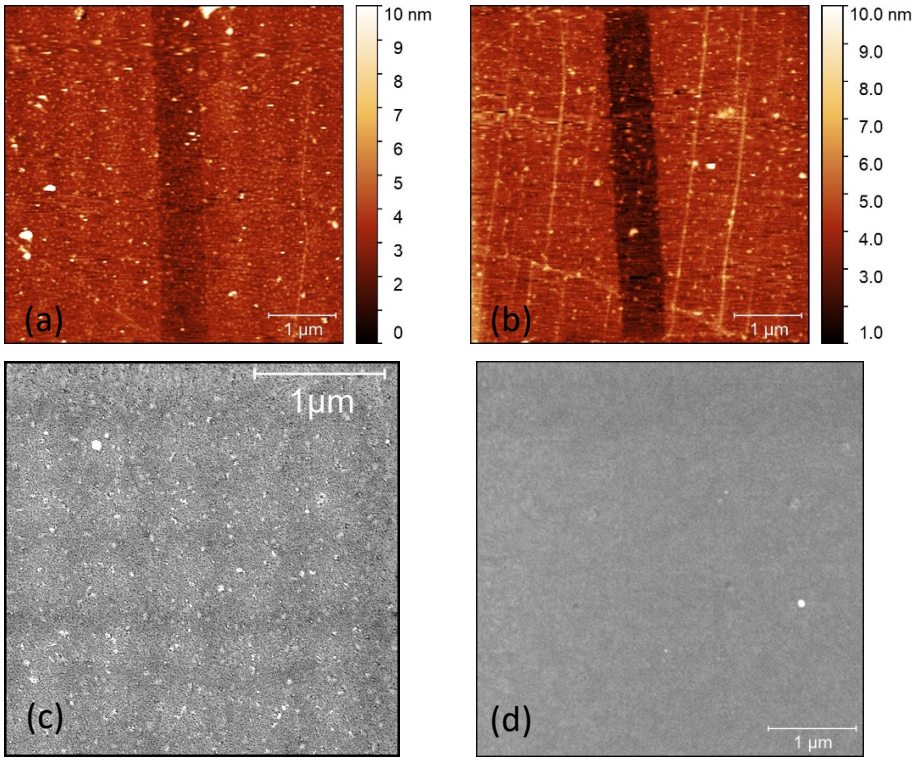

Figure S7.1. The devices annealed with 500 nm (a, c) and 200 nm (b, d) scanning steps are analysed with AFM (a, b) and SEM (c, d). It is clear that the 500 nm scanning step results in uneven annealing. The surface roughness (RMS square) of 740 pm and 600 pm is estimated for 500 nm and 200 nm scanning steps, respectively. Note, the wrinkles are excluded from the analyses. The gap in the device centre (a, b) corresponds to the gap between the graphene contacts. This gap is not detectable with SEM.

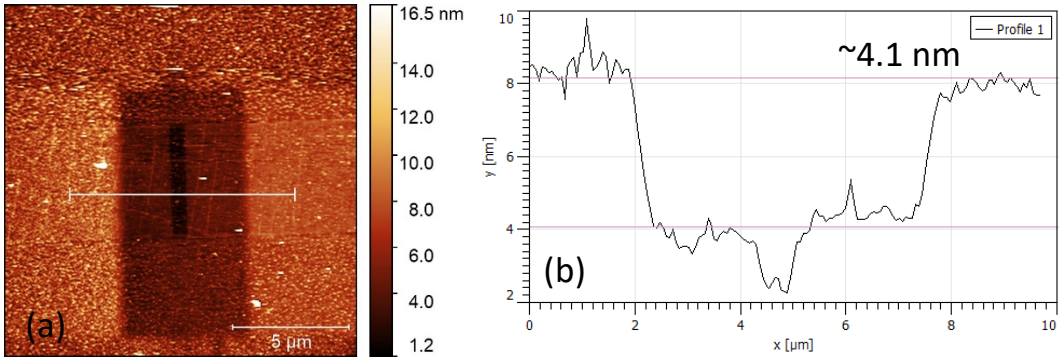

Figure S7.2. AFM measurements of the device after laser annealing with a 200 nm scanning step. (a) AFM image and corresponding cross section (b). The film thickness is reduced by ~4.1 nm.

S8. $PdSe_2$ FET devices with gold electrodes

A continuous $PdSe_2$ film was transferred on the array of gold contact pads. Next, the devices were mechanically separated from each other using a probe tip. Then the device channels were

fully defined by laser exposure with high power of 7.8 mW. One sample was further modified using laser power exposure with 1.8 mW and 200nm step. The sample after the channel annealing exhibits ~4 times improvement in conductivity and almost twice higher mobility.

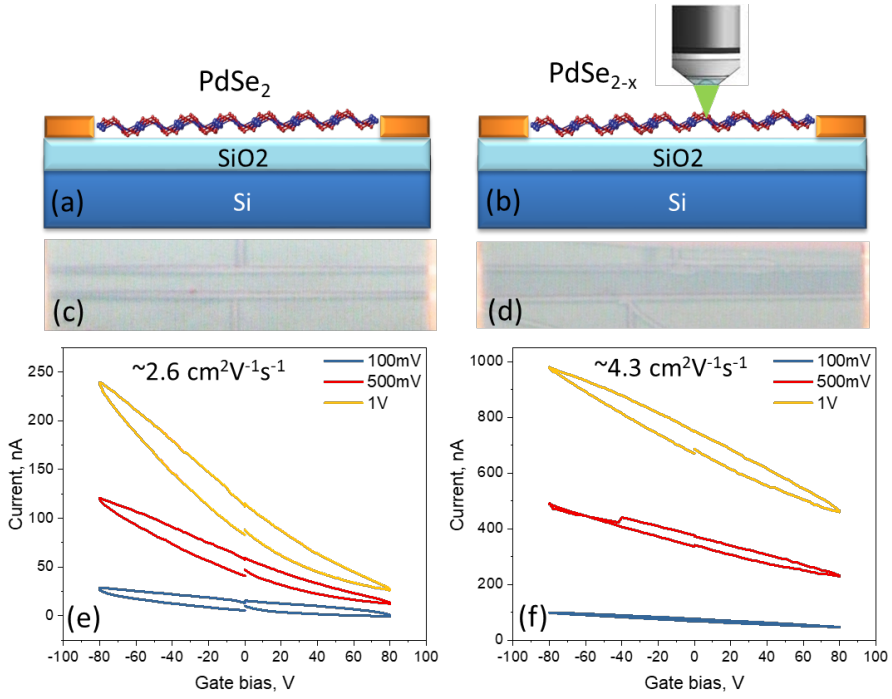

Figure S8.1. Electrical characterisation of the $PdSe_2$ FET devices with gold contacts before and after laser modification. (a, b) Schematic side view of the samples. (c, d) Optical microscopy image of the samples after $PdSe_2$ channel fabrication and after laser modification for (d). The channel length is 50 µm and the resultant channel widths are 2.6 µm and 3.22 µm, respectively. (e, f) Transfer curves for unmodified and annealed FET devices.

It is interesting to demonstrate that the patterning with high laser power can be further used to create the gap in the device channel. For this purpose, we perform a laser cut in the device channel and analyse the device conductivity. Compared to the initial device described above the current is less than 10 nA for applied 5 V source-drain bias, which is in contrast to 100 nA observed for 1 V source-drain bias.

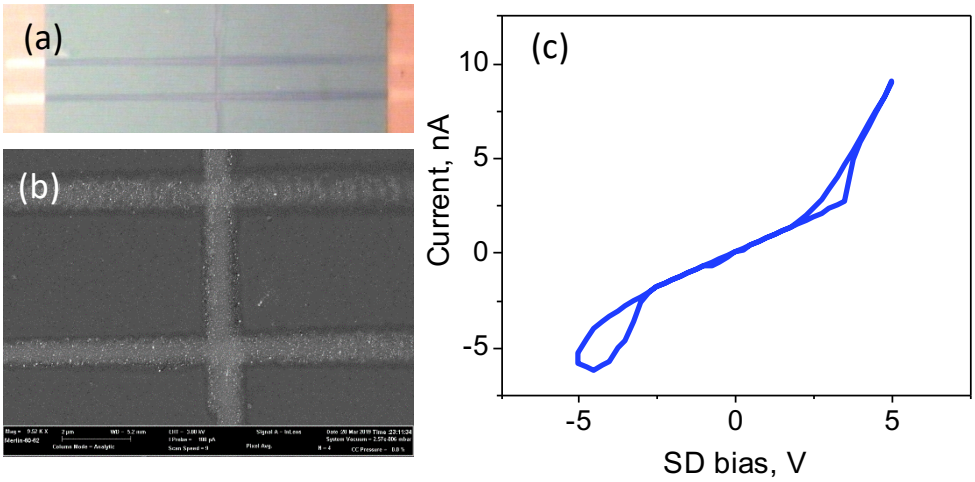

Figure S8.2. Electrical characterisation of the $PdSe_2$ FET devices with laser cut gap in the channel. (a, b) Optical microscopy image and SEM. (c) I-V curve of the device with the laser patterned gap.

To understand the interface formed between initial $PdSe_2$ and laser modified $PdSe_2$ material, we perform laser annealing of the half of the channel, as can be seen by darker contrast in the optical microscopy image (inset Fig. S7.3a). As discussed in the main text, after the laser annealing the $PdSe_2$ peak intensity is reduced. The IV characteristic shows Ohmic behaviour for the final device which is in good agreement with expected interface properties between p-doped $PdSe_2$ area and metallic $PdSe_{2-x}$ phase. Gate-dependent measurements are typical of $PdSe_2$ channel consistent with high resistance of the unpatented area that is expected to dominate the device performance.

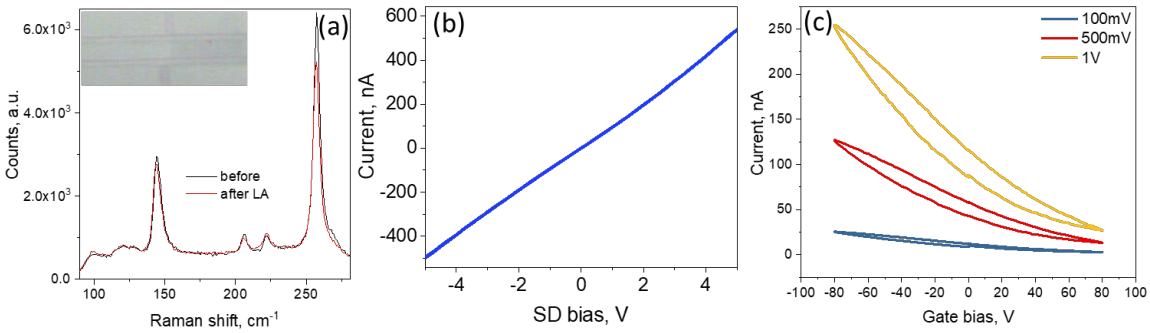

Figure S8.3. Electrical characterisation of the $PdSe_2$ FET device with half patterned channel. (a) Raman spectra for areas before and after laser annealing. Inset shows optical microscopy image of the final device. (b, c) Typical transfer curves of the device.

S9. Influence of thermal annealing

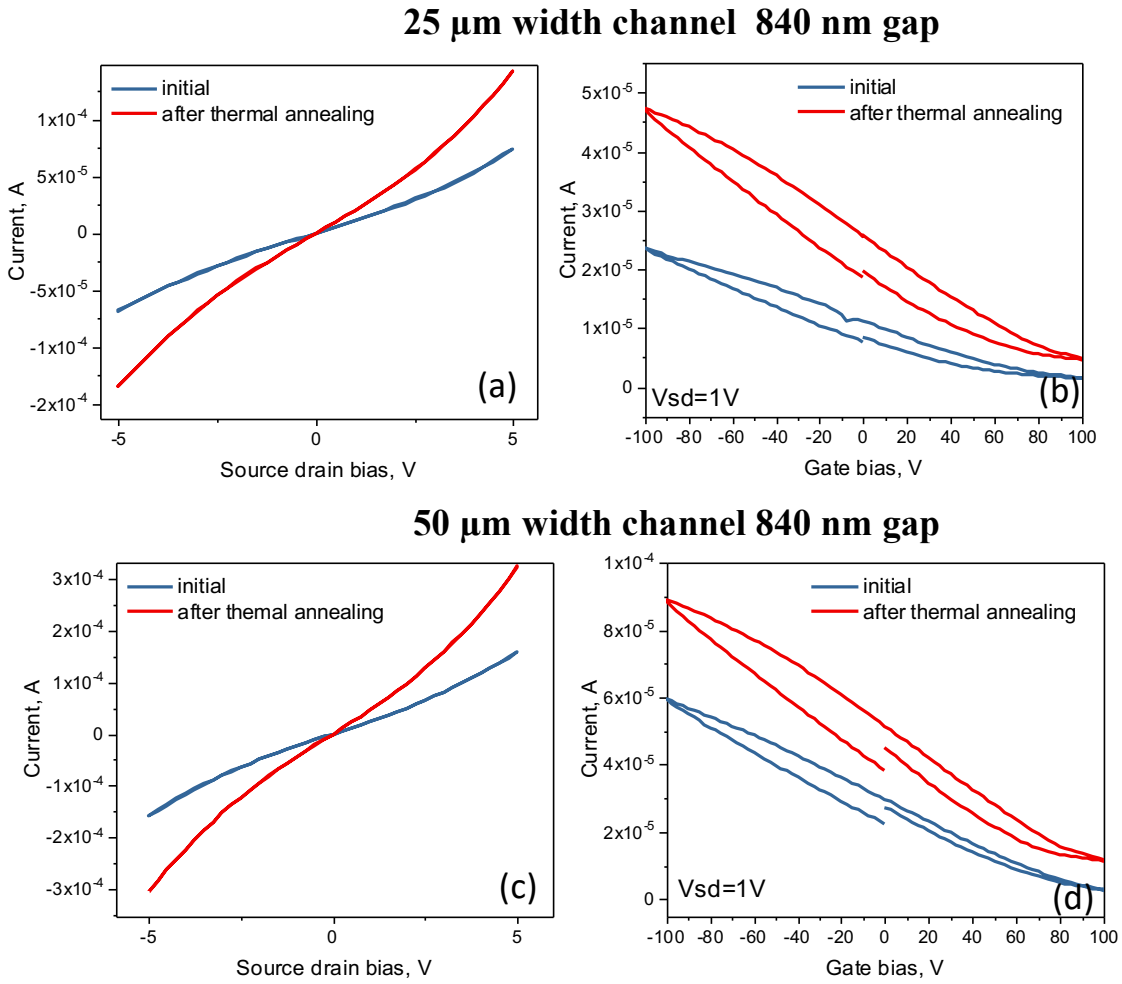

Figure S9. Electrical characterisation of the $PdSe_2$ FET devices before and after thermal annealing in high vacuum for 12h. The measurements are performed for the devices with 25 25 µm (a,b) and 50 µm (c,d) width channel.

S10. Device statistics

Devices with varying gap of graphene electrodes

Table S1. Mobility summary for devices with varying gap.

Graphene contact gap	**Initial mobility, ($cm^2V^{-1}s^{-1}$)**	**Mobility after laser annealing, ($cm^2V^{-1}s^{-1}$)**	**Mobility ratio**
475nm gap	0.0651	0.4406	7
840nm gap	0.50	1.4711	3
1.2um gap	0.12	2.16	18

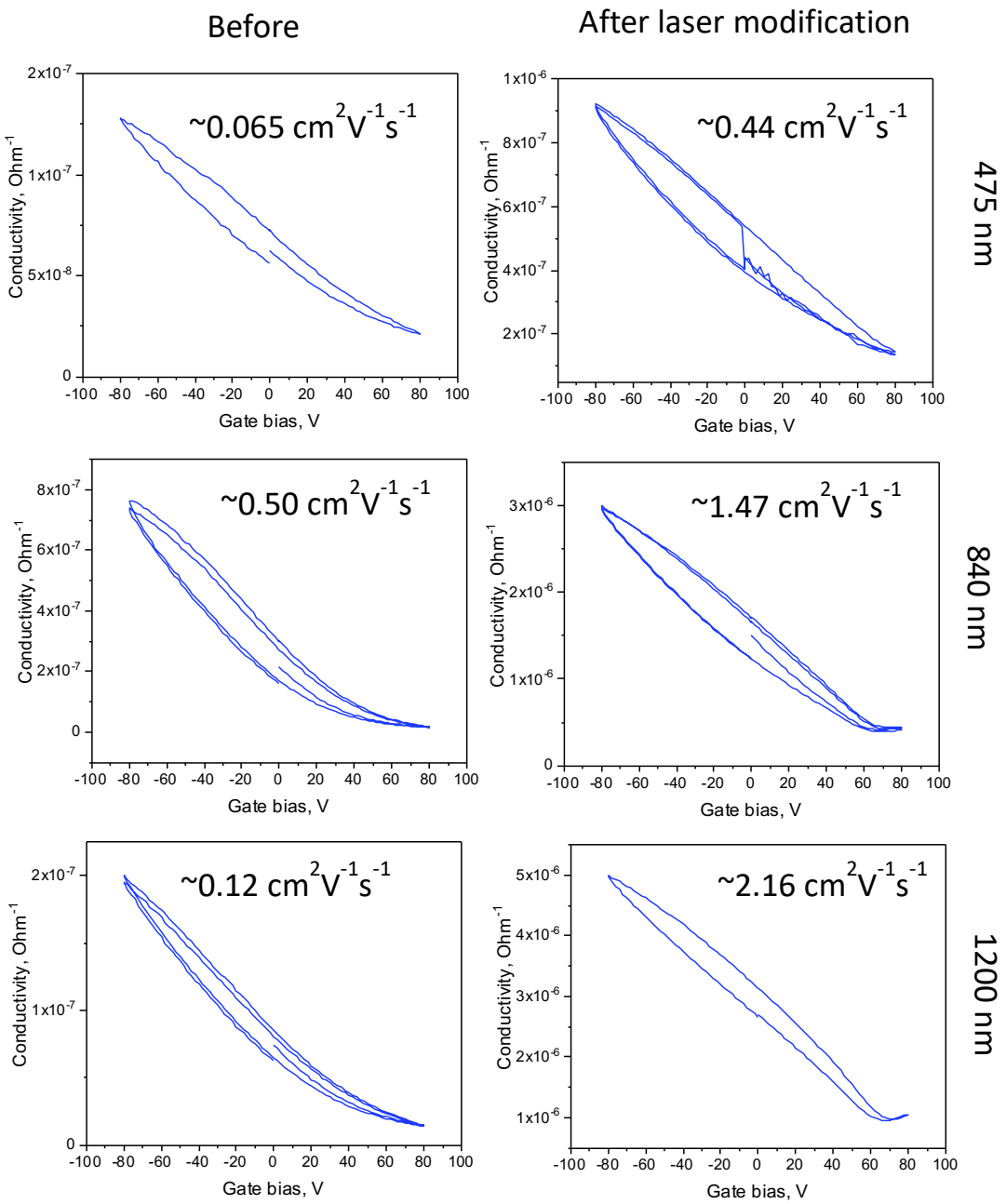

Figure S10.1. Electrical characterisation of the devices with varying gap size between the graphene electrodes. The device performance is analysed before and after laser modification with 1.8 mW power and 200 nm step.

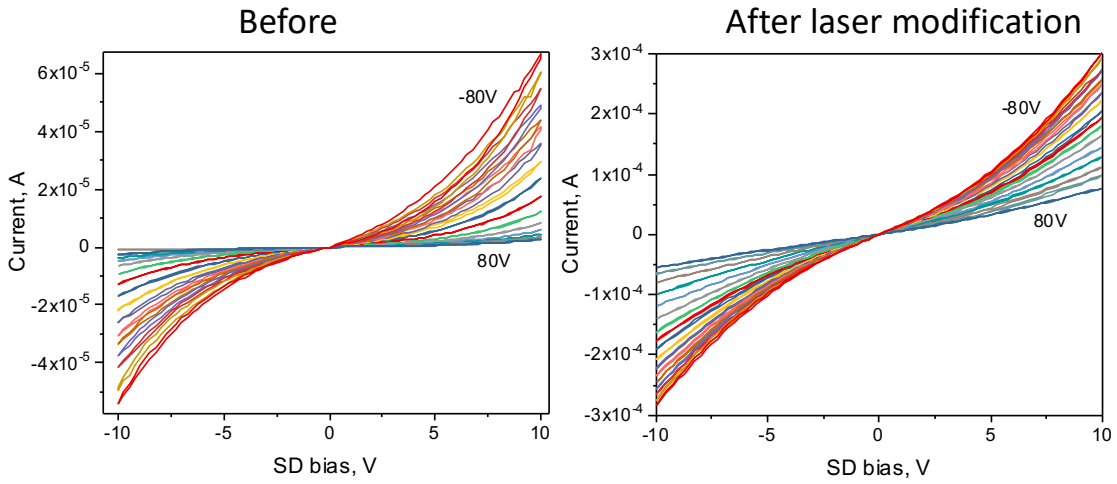

Figure S10.2. Electrical characterisation of the device with 840nm gap before and after laser modification (1.8 mW power and 200 nm step). The measurements are performed with varied back gate bias in the range of -80 to 80V.

Devices with 1.2 µm gap

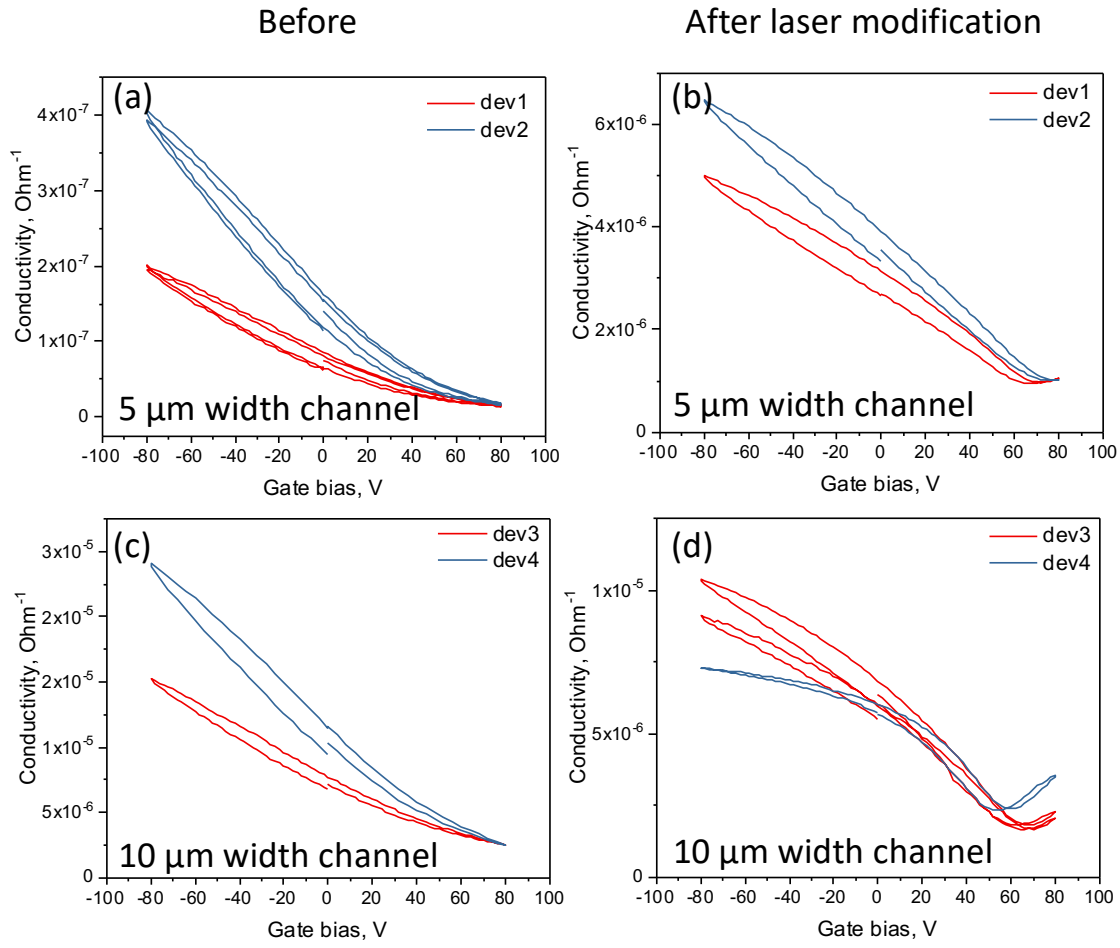

Figure S10.3. Electrical characterisation of the devices with 1.2 µm gap between graphene electrodes and varying width of the graphene electrodes, namely 5 µm (a, b) and

10 µm (c, d). The device performance is analysed before and after laser modification with 1.8 mW power and 200 nm step.

Table S2. Mobility summary for devices with 1.2 µm gap.

Device number	**Initial mobility, ($cm^2V^{-1}s^{-1}$)**	**Mobility after laser annealing, ($cm^2V^{-1}s^{-1}$)**	**Mobility ratio**
dev1	0.12	2.16	18
dev2	0.27	3.03	11.2
dev3	0.19	7.24	38
dev4	0.33	8.1	24.5

Devices with multiple laser exposure

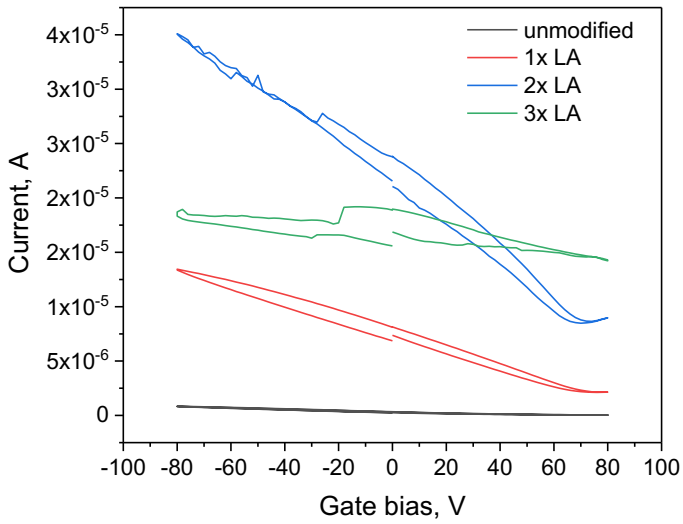

Figure S10.4. Electrical characterisation of the device with multiple laser exposures. It is clear that the second laser exposure further improves conductivity, while the third laser exposure results in degradation, which might be due to material segregation and NP formation.

S11. MoS_2 and WS_2 laser-induced degradation

It is interesting to compare the laser sensitivity of the $PdSe_2$ material to other well-studied TMDC materials such as MoS_2 and WS_2. We observe similar laser sensitivity in case of monolayer WS_2 material, where 1.8 mW laser exposure results in the local material modification, as confirmed by SEM results. Interestingly, monolayer MoS_2 material requires much higher laser powers to induce observable material transformation. In fact, the laser power of as high as 7.8 mW is needed. This is in stark contrast with $PdSe_2$ material, where the full material degradation is observed at this laser power.

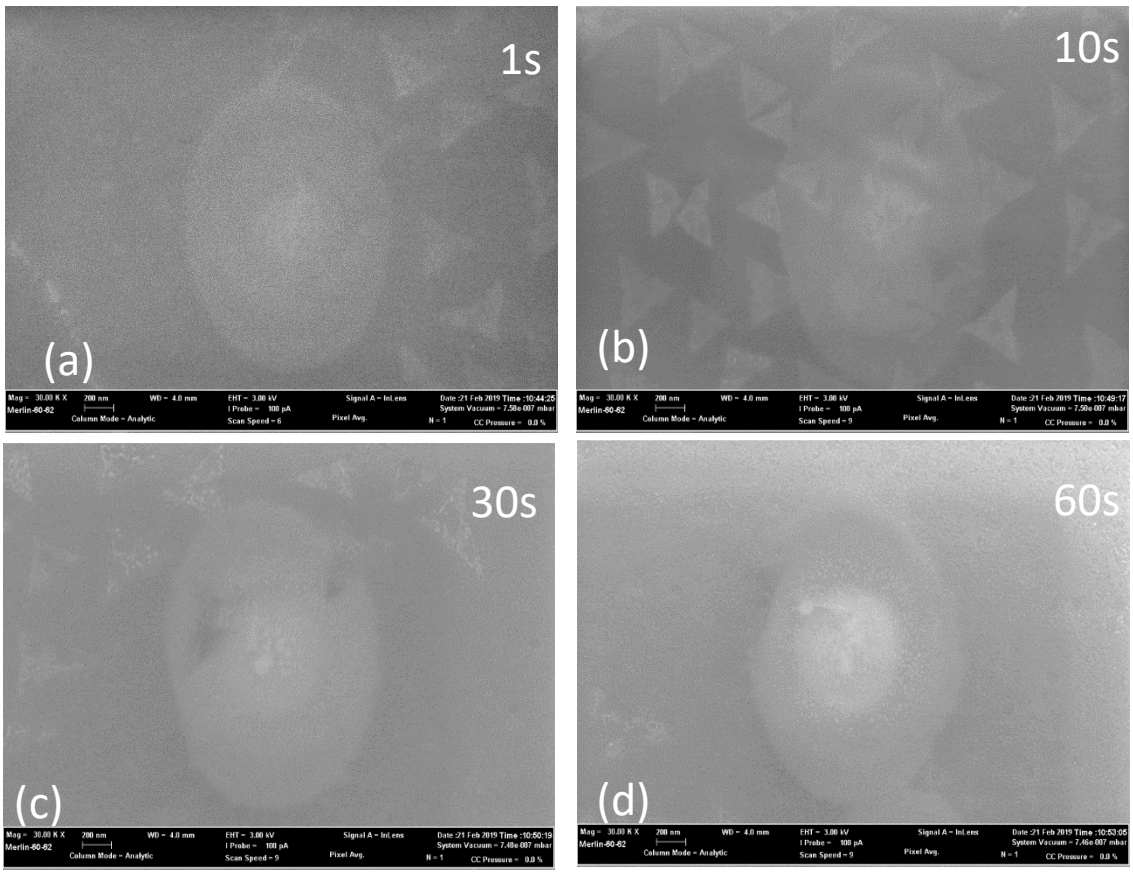

Figure S11.1. MoS_2 sensitivity to laser exposure. The material is exposed with 7.8 mW during varying time of 1s (a), 10s (b), 30s (c) and 60s (d). Interestingly, the material modification with the laser powers of 0.6, 1.8 and 3.5 mW is not detected with SEM.

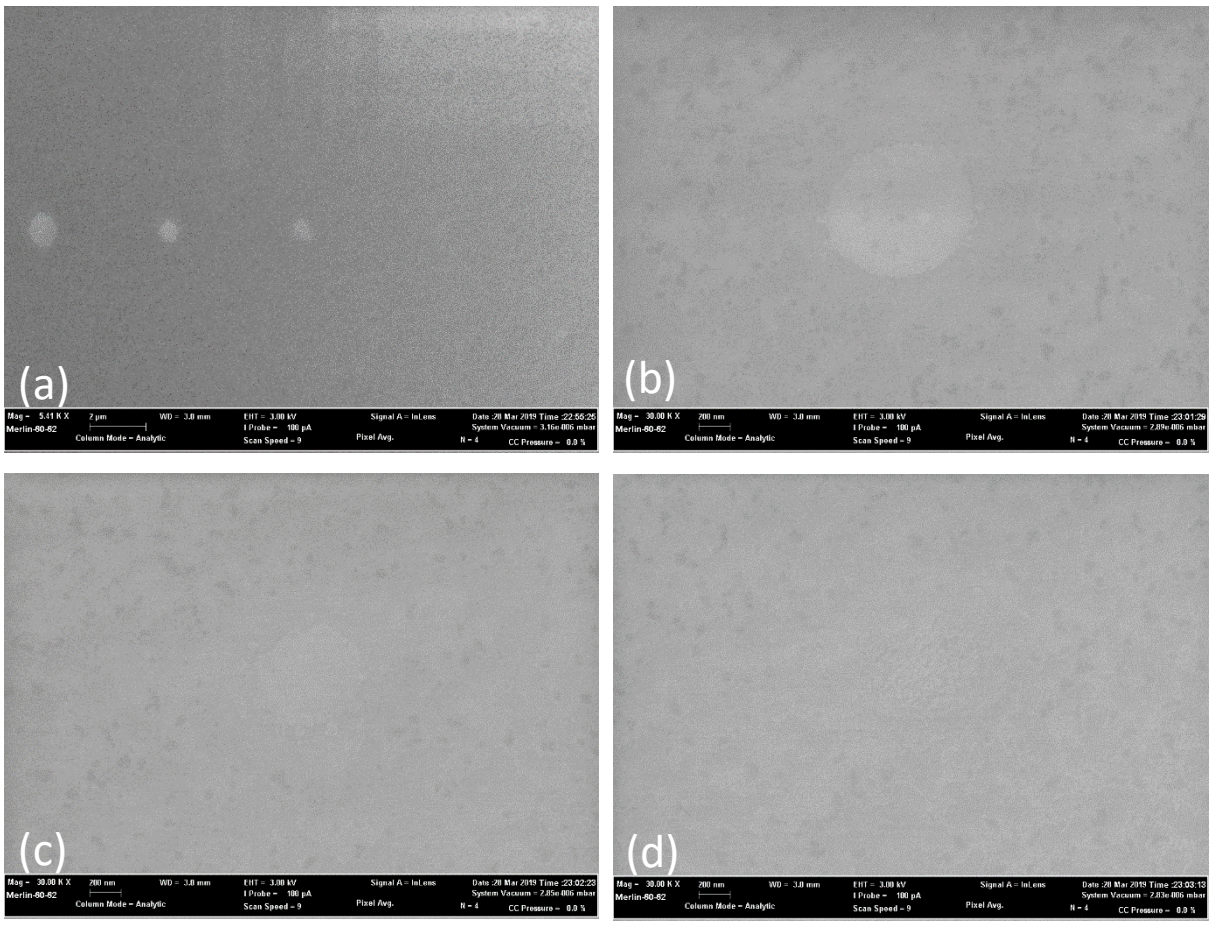

Figure S11.2. WS_2 sensitivity to laser exposure. The material is exposed for 1s with varying laser power of 0.6, 1.8, 3.5 and 7.8 mW (a), corresponding high magnification images (b-d).

References:

1. Ryu, G. H.; Zhu, T.; Chen, J.; Sinha, S.; Shautsova, V.; Grossman, J. C.; Warner, J. H. Striated 2D Lattice with Sub-nm 1D Etch Channels by Controlled Thermally Induced Phase Transformations of PdSe2. *Adv. Mater.* **2019**, *1904251*, 1904251.